CESAM - Coded excitation scanning acoustic microscope

Meriläinen, Antti

2021-07-01

Meriläinen , A , Hyvönen , J T J , Salmi , A & Haeggström , E 2021 , ' CESAM - Coded excitation scanning acoustic microscope ' , Review of Scientific Instruments , vol. 92 , no. 7 , 074901 . https://doi.org/10.1063/5.0047351

http://hdl.handle.net/10138/346233
https://doi.org/10.1063/5.0047351

unspecified
publishedVersion

Review of Scientific Instruments

CESAM—Coded excitation scanning acoustic microscope

Cite as: Rev. Sci. Instrum. **92**, 074901 (2021); https://doi.org/10.1063/5.0047351
Submitted: 12 February 2021 . Accepted: 01 July 2021 . Published Online: 16 July 2021

Antti Meriläinen, Jere Hyvönen, Ari Salmi, and Edward Hæggström

Review of Scientific Instruments ARTICLE scitation.org/journal/rsi

CESAM—Coded excitation scanning acoustic microscope

Cite as: Rev. Sci. Instrum. 92, 074901 (2021); doi: 10.1063/5.0047351
Submitted: 12 February 2021 • Accepted: 1 July 2021 •
Published Online: 16 July 2021

Antti Meriläinen,[a] Jere Hyvönen, Ari Salmi, and Edward Hæggström

AFFILIATIONS

Electronics Research Laboratory, Department of Physics, University of Helsinki, Gustaf Hällströmin katu 2, FIN 00560 Helsinki, Finland

[a]Author to whom correspondence should be addressed: antti.merilainen@helsinki.fi

ABSTRACT

Scanning acoustic microscopy (SAM) finds use across many disciplines, e.g., biology, industrial quality control, and materials science, thanks to its unique ability to quantify mechanical sample properties combined with its high resolution. However, such imaging is often slow, especially if averaging is necessary. We present a Coded Excitation Scanning Acoustic Microscope (CESAM) that employs coded signals and show that it produces images of higher signal-to-noise ratios (SNRs) than the classical SAM in a comparable measurement time. The CESAM employs coded signals instead of the short bursts used in traditional SAMs, and we employ both linear and non-linear frequency modulation. Our results show that compared to the SAM approach, this modulation increases the SNR by 16.3 dB (from 39.9 to 56.2 dB) and reduces the echo duration by 26.7% when we employ a linear chirp to the transducer with a nominal bandwidth of 130–370 MHz. Driving the transducer with a broader bandwidth signal using non-linear chirps (100–450 MHz), we obtained a SNR increase of 10.3 dB and a reduced echo duration of 70.5%. The shorter echo duration increases z-resolution, whereas the lateral resolution remains limited by the wavelength. Finally, we show that by using these coded signals, one can obtain enhanced image quality relative to the standard actuation of the same measurement time. Our results have potential to invigorate the field of acoustic microscopy, especially with samples where the enhanced SNR and/or contrast-to-noise ratio is crucial for image quality.

INTRODUCTION

Acoustic microscopy is an established technique, originated in the 1970s,[1] which has found use in many fields, e.g., biomedical research and industrial quality assurance.[2–4] Scanning acoustic microscopy (SAM) provides images of microstructures where the contrast arises from mechanical properties, e.g., elasticity and acoustic impedance.[2,5] Recent development work has focused on reducing measurement time[6] and on increasing the bandwidth and reliability[2] of SAM transducers. Conventional SAM systems recorded a video signal maximum for each measured point, losing the phase information of the echoes. Modern systems are often time-resolved, meaning that they record the whole RF signal, which allows digital post-processing. Chen *et al.* applied an acoustic microscope and V(z, t)-measurements to study the properties of thin plates. Their setup operated at low frequencies (15–35 MHz) and was time-resolved.[7,8] Acoustic microscopy was applied by Vogg *et al.* and Ross *et al.* with a conventional SAM operating up to GHz frequencies.[4,9] They studied microelectronics with different frequencies and discussed the benefits of ultra-high frequency SAM. Their setup was not time-resolved and included a pre-digitation processing that lost the phase information of the signals. A high-frequency (500 MHz) time-resolved system was presented by Rohrbach *et al.* to study biological tissues quantitatively.[2]

Other modalities for non-destructive testing (NDT) and imaging include photoacoustics, optical microscopy, atomic force microscopy (AFM), and x-ray imaging. The largest difference between SAM and these other modalities is the contrast mechanism: SAM measures the mechanical properties of samples by inferring the acoustic impedance, whereas the other modalities measure either optical properties (photoacoustics and optical microscopy) or density (x-ray imaging). AFM also measures mechanical properties rather slowly and from a small area. Contacting operation (tapping mode) is required to extract the mechanical parameters of a sample.[10] There exists a large area AFM that employs multiple cantilevers.[11]

Traditionally, a SAM features a pulser or a signal generator that generates a short burst, which provides high temporal resolution. Short bursts are broadband, and thus, their amplitude needs to be high to contain enough energy inside the transmission band. The thin piezostructures used in SAM transducers limit the applicable signal amplitude (risk of transducer breakage).[12]

To obtain large excitation energy without breaking the transducers, one should spread the signal energy in time. This cannot be done with a traditional burst excitation without losing time resolution,[13] and hence, coded signals are required. Coded signal excitation decreases the measurement time (no averaging needed), enhances the signal-to-noise ratio (SNR),[13–15] and allows bandwidth tuning.[16,17] Since the SNR is directly proportional to the employed code length, the coded excitation provides a way to avoid signal averaging.[18] For high-frequency SAM devices, coded signals have been tested with fixed codes.[14] At lower frequencies, chirp excitation has been used,[19,20] and there are studies on the imaging fidelity of acoustic microscopes.[4] The current state-of-the-art of commercial and custom-built SAM devices is described in Refs. 2 and 4, respectively.

New computer hardware allows us now to enhance the work done in the interdigital transducer (SAW-filter) field, whereas in the 1980s, hardware structures[14,21] were used for correlator-based signal compression. The major difference between now and then is that previously one had to manufacture a dedicated hardware structure for every code and the user had to manually exchange this structure if the codes were to be changed. This is no longer necessary: the codes can be implemented and changed on-the-fly using software.

In this study, we use arbitrary coded signals[22] in our Coded Excitation Scanning Acoustic Microscope (CESAM). We test linear and non-linear chirps. A significant advantage of our proposed method is that it allows simultaneous reduction of echo duration and an increased SNR compared to burst excitation. Most importantly, this improvement should be possible without sacrificing imaging fidelity.

MATERIALS AND METHODS

CESAM hardware

We built a CESAM on a passively isolated optical table (SDA7590 frame, B7590L plate, Thorlabs, New Jersey, United States) to minimize the effect of environment vibrations. The instrument features a 250 MHz transducer (bandwidth: 225 MHz, 60°, and NA: 0.5; Sa#10-17#0010, Kibero GmbH, Saarbrücken, Germany) that was connected to a goniometer (GN2/M, Thorlabs, New Jersey, United States) and a linear stage (MTS 25/M-Z8, controller KDC101, Thorlabs, New Jersey, United States). The samples were attached to a custom-made sample holder that was bolted to a 2D linear stage (MLS203-1, controller BBD202, Thorlabs, New Jersey, United States) and a goniometer (GN2/M, Thorlabs, New Jersey, United States). A detailed list of equipment is presented in supplementary material 1 (Table I). The z-direction movement, used to find the correct working distance in the beginning of the measurement, was controlled with a linear stage (MTS25/M-Z8, Thorlabs, New Jersey, United States). The schematic of the CESAM is presented in Fig. 1.

The signals were generated using a Peripheral Component Interconnect Express (PCIe) arbitrary waveform generator (AWG, M4i.6631-x8, Spectrum Instrumentation GmbH, Grosshansdorf, Germany) and were subsequently frequency doubled (ZX90-2-13-S, Mini Circuits, New York, United States) and amplified (30 dB; ZHL-42W, Mini Circuits, New York, United States) before forwarding them to a custom-built RF switch (see supplementary material 2) that performed the pulse-echo measurement utilizing the transducer. The Rx signals received by the switch were pre-amplified (23 dB; ZFL-1000LN+, Mini Circuits, New York, United States) and recorded with a PCIe digital oscilloscope (M4i.2233-x8, Spectrum Instrumentation GmbH, Grosshansdorf, Germany). The key parameters of acquisition are listed in Table I.

The measurements were performed by triggering the AWG with a microcontroller development board (Arduino Due, Arduino

TABLE I. Key data acquisition parameters.

Tx	Tx sampling frequency	1.25 GS/s
	Tx signal length	24 ns (burst)/1 μs (chirps)
	Tx DAC resolution	16 bit
Rx	Rx sampling frequency	2.5 GS/s
	Rx signal length	6.55 μs
	Rx ADC resolution	8 bit
Signal processing	Time gate (first–second lens echo)	1.2 μs (after cross-correlation)
	Variable type	32 bit floating point (IEEE 754)
Scanning	Scan range	2 × 2 mm^2 (used) 110 × 75 mm^2 (max)
	Scan velocity	12 mm/s (used), 100 mm/s (max)
	Scan increment	2 μm
	Scan on-the-fly	Yes
	Single shot	Yes
	Scan time	10 min/1 Mpixel, 2 μm steps

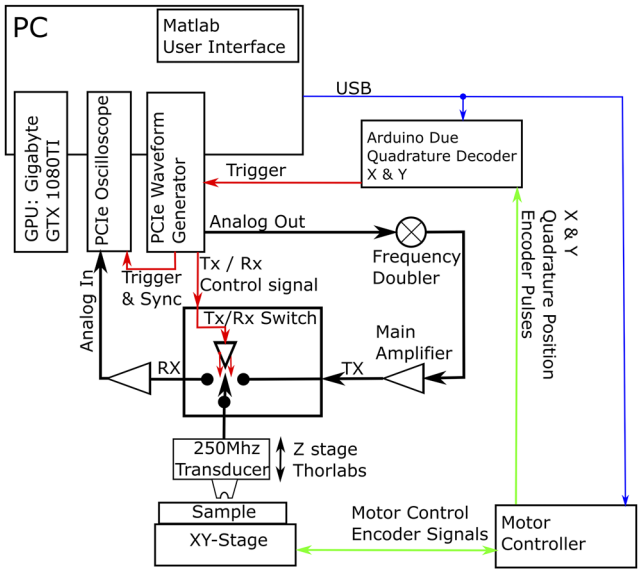

FIG. 1. Schematic of the CESAM. A personal computer (PC) controlled both the digital oscilloscope that collects data and an arbitrary waveform generator that forwards the signals after amplification to a custom-made RF switch necessary for pulse-echo measurements. The sample was scanned with a 2D linear stage, and the transducer–sample distance was controlled with a linear stage. The different colors describe different types of signals: red corresponds to digital signals, black to analog signals, blue to universal serial bus (USB), and green to differential digital signals.

LLC, Italy) that tracked the position of the 2D stage by counting the quadrature encoder pulses (50 nm/pulse). The Arduino board sent a trigger signal when the translation stage had traveled a pre-set distance. The data acquisition was triggered by the AWG.

Coded signals

We used Matlab (2017a, Mathworks, Massachusetts, United States) to generate the coded signals. The codes included a linear frequency modulation (LFM / chirp) from 130 to 370 MHz and two different non-linear frequency modulation (non-LFM) codes from 130 to 370 MHz and from 100 to 450 MHz, respectively. Non-linear FM codes were chosen since the signal energy is distributed across a broader frequency band (Fig. 2). For burst excitation, we transmitted six cycles at 250 MHz, 8.0 Vpp (22 dBm), and a signal length of $T = 24$ ns. The amplitudes and duty cycles were chosen in the way that the manufacturer's specifications for the transducer were not exceeded. All transmit signals were amplitude modulated with a Gaussian envelope ($\sigma = 200$ ns for coded signals and $\sigma = 4.8$ ns for the burst) to avoid temporal side lobes. The amplitude modulation (AM) is

$$A(t) = e^{\frac{-\left(t-\frac{T}{2}\right)^2}{2\sigma^2}}, \quad t = 0 \rightarrow T, \quad \sigma = \frac{T}{5}, \tag{1}$$

where T is the signal length and t is the time. The burst signal is

$$Tx_{Burst}(t = 0 \rightarrow T) = A_{Burst}(t)\sin(2\pi t f_{Center}), \tag{2}$$

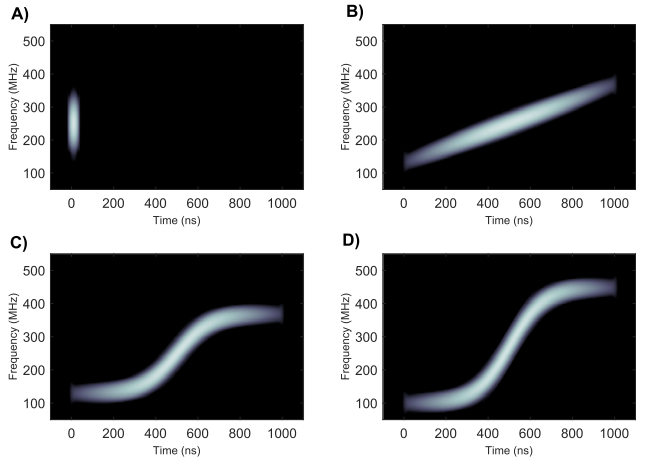

FIG. 2. Spectrograms of different Tx signals: (a) burst excitation (six cycles, 250 MHz), (b) linear chirp (130–370 MHz, 1 μs), (c) non-linear chirp (130–370 MHz, 1 μs), and (d) non-linear chirp (100–450 MHz, 1 μs).

where f_{Center} is the center frequency (250 MHz) and A_{Burst} is the burst amplitude.

Generally, signals for coded excitation should be as long as possible. Here, we were limited by the transducer's acoustic delay line since our RF switch did not allow simultaneous Tx and Rx operation. The delay line of our transducer was 1 μs, which is used as the signal length. In general form, the FM-chirp is

$$Tx(t = 0 \rightarrow T) = A(t)\cos(\Phi(t)), \tag{3}$$

$$\frac{d\Phi(t)}{dt} = 2\pi f(t), \; f(t) = f_{Center} + f_{Mod}(t), \tag{4}$$

where $\Phi(t)$ is the instantaneous phase, f_{Center} is the center frequency of the signal, and $f_{Mod}(t)$ is the frequency modulation. Table II summarizes the equations for different signals.

The spectrograms of all Tx signals are plotted in Fig. 2. Note that $f_{Center} = 250$ MHz for the burst and for the 130–370 MHz LFM and non-LFM signals, whereas for the 100–450 MHz non-LFM signal, $f_{Center} = 275$ MHz.

Samples

We used a USAF 1951 (R1DS1P, Thorlabs, New Jersey, United States) resolution sample (group 7 elements) to determine the

TABLE II. Tx-signal specifications.

Signal type ($f_{Start} - f_{Stop}$)	Frequency modulation phase
Burst 6 cyc., 250 MHz	None
LFM chirp, 130–370 MHz	$\Phi_{LFM}(t) = 2\pi\left(\frac{k}{2}t^2 + f_{Start}t\right)$
Non-LFM chirp, 130–370 MHz Non-LFM chirp, 100–450 MHz	$\Phi_{non-LFM}(t) = 2\pi t f_{Center} + T\frac{f_{Stop}-f_{Start}}{2}\ln\left[\frac{\cosh\left(2\pi\frac{t}{T}-\pi\right)}{\cosh(\pi)}\right]$

resolution of the microscope. To identify the presence of possible distortion effects, we used a 100 μm grid sample (R1L3S3P, Thorlabs, New Jersey, United States) and imaged an area of 4 mm^2 (see supplementary material 4). Both samples used to characterize the instrument were metallic (chromium) thin film structures (120 nm thick) on a soda lime glass substrate. The linewidth and spacing for USAF 1951 group 7 elements were 3.91, 3.48, 3.10, 2.76, 2.46, and 2.19 μm from elements 1 to 6, respectively. Finally, to show the performance of our device in a real-world scenario, we measured a pure and polished polycrystalline copper sample.

All measurements were performed in deionized water immersion at room temperature.

Signal processing

The digitized Rx signals were read from the oscilloscope to the GPU memory (GTX 1080Ti, Gigabyte Technology, New Taipei City, Taiwan). We used GPU parallelization to accelerate the cross-correlation of the Tx and Rx signals since each scan comprised thousands of independent A-lines that could be analyzed separately. This sped up the data analysis by a factor of ~100 compared to calculations performed only on the CPU. The data were subsequently analyzed with a custom-made data analysis algorithm (supplementary material 3) using Matlab.

The used cross-correlation function is

$$[Signal_{Tx} \star Signal_{Rx}](t) = \int_{-\infty}^{\infty} Signal_{Tx}(t-\tau) Signal_{Rx}(t) d\tau, \quad (5)$$

where $Signal_{Tx}$ and $Signal_{Rx}$ are the transmitted and received signals, respectively.

We determined the signal-to-noise ratio (SNR) and contrast-to-noise ratio (CNR) for the signals as follows:

$$SNR_{dB} = 20\log_{10}\left(\frac{\overline{Echo\ Amplitude}}{\overline{Noise\ Floor}}\right), \quad (6)$$

$$CNR_{dB} = 20\log_{10}\left(\frac{Contrast}{\sigma_{Pixel\ Amplitudes}}\right) = 20\log_{10}\left(\frac{1}{\sigma_{Pixel\ Amplitudes}}\right), \quad (7)$$

where $\sigma_{\text{pixel amplitudes}}$ is the standard deviation of the amplitudes of pixels in an area with no identified features. The contrast is one since the signal amplitudes are normalized. We used USAF 1951 C-Scan data to determine CNRs.

RESULTS

Cross-correlated signals obtained with the three different codes and one obtained by burst excitation (without cross-correlation) are shown in Fig. 3. To allow fair amplitude comparison between the signals, we normalized the cross-correlated signals so that the burst maximum amplitude was 1 [Fig. 3(a); supplementary material 5]. Figure 3(e) shows the power spectrum of echoes that have been normalized by the pulse energy. The energy of the received burst signal (black line) is significantly lower than that of the chirp signals since the burst duration is much shorter than the duration of the chirps.

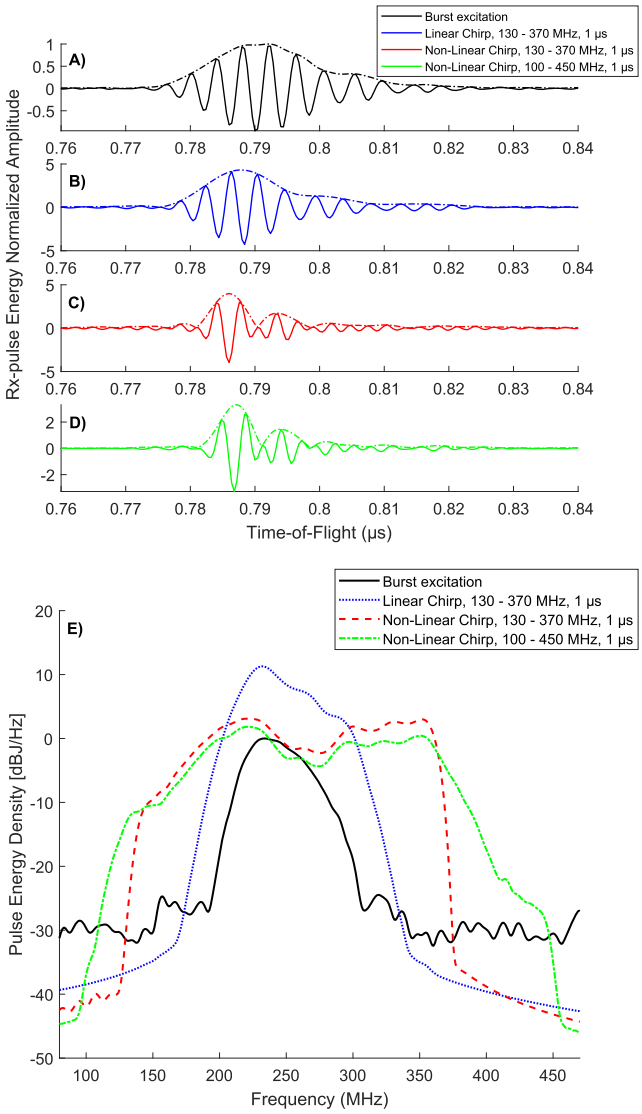

FIG. 3. Received signals and their envelopes obtained by different methods: (a) traditional burst excitation at 250 MHz (six cycles), (b) cross-correlated linear chirp (130–370 MHz; burst length, 1 μs), (c) cross-correlated non-linear chirp (130–370 MHz; burst length, 1 μs), (d) cross-correlated non-linear chirp (100–450 MHz; burst length, 1 μs), and (e) spectra of the received signals [color coding as in (a)–(d)]. The time-of-flight axis in (a)–(d) is set to begin at the first lens echo. Amplitudes are normalized to the energy so that the burst maximum amplitude is 1.

We calculated the SNR at each imaged point for all signals. The results given in Table III indicate that coded signals increase the SNR and decrease the echo width compared to burst excitation that serves as reference.

To demonstrate imaging fidelity, we imaged a USAF 1951 resolution test sample (Fig. 4). Improved image quality is seen (less noise, higher contrast, and more resolution), especially in the line

TABLE III. Results obtained with different excitation signals.

Signal type	Mean SNR (dB) ± standard deviation	SNR increase (dB)	CNR (dB)	CNR increase (dB)	Width of echo (ns)	Decrease in the pulse width (%)
Burst 6 cyc., 250 MHz	39.9 ± 0.4	0	18.9	0	16.8	0
Linear chirp, 130–370 MHz	56.2 ± 0.8	16.3 ± 0.8	28.2	9.3	12.3	26.7
Non-linear chirp, 130–370 MHz	47.5 ± 0.2	7.6 ± 0.2	26.9	8	5.2	69
Non-linear chirp, 100–450 MHz	50.2 ± 0.4	10.3 ± 0.2	27.8	8.9	5.0	70.5

across the elements (Fig. 5). Furthermore, we scanned a distortion test sample (supplementary material 4) to demonstrate that we can scan large areas without image distortion. This was an issue in early SAM studies.[5] Our device employs a triggering system that actively listens to encoder pulses from the translation stages.

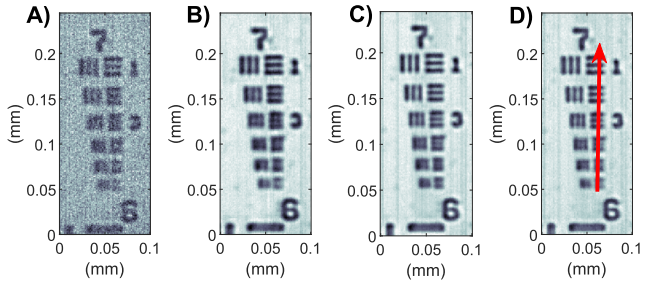

FIG. 4. Amplitude C-scan of a USAF 1951 resolution sample (group 7 elements): (a) traditional burst excitation at 250 MHz (six cycles), (b) linear chirp excitation (130–370 MHz; burst length, 1 μs), (c) non-linear chirp excitation (130–370 MHz; burst length, 1 μs), and (d) non-linear chirp excitation (100–450 MHz; burst length, 1 μs).

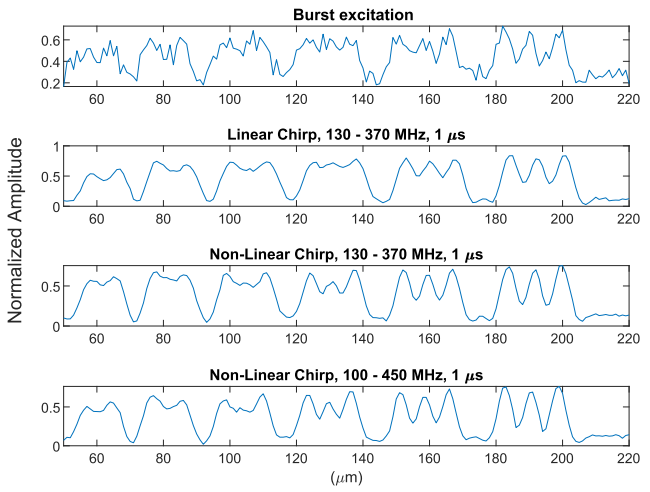

FIG. 5. Amplitude plots obtained by different methods along the arrow in Fig. 4(d).

In Fig. 6, B-scans are plotted along the arrow shown in Fig. 4(d) for each used signal. This figure shows enhanced Z-resolution due to wideband coded excitation when compared to burst excitation. The increase in the bandwidth reduces the pulse length as expected. The grayscale background represents the echo envelope, and the red line is the maximum of the echo signal.

To demonstrate the real-life functionality of our device, we measured a copper sample (Fig. 7). The coded signals created an image with a higher contrast-to-noise ratio (CNR) than that obtained by the traditional excitation.

DISCUSSION

In this paper, our aim was to show that a CESAM produces higher quality images in the same measurement time compared to traditional burst excitation. Care was taken to ensure fair comparison between the imaging modalities. Fair comparison means the same machine, the same sample, the same measurement time

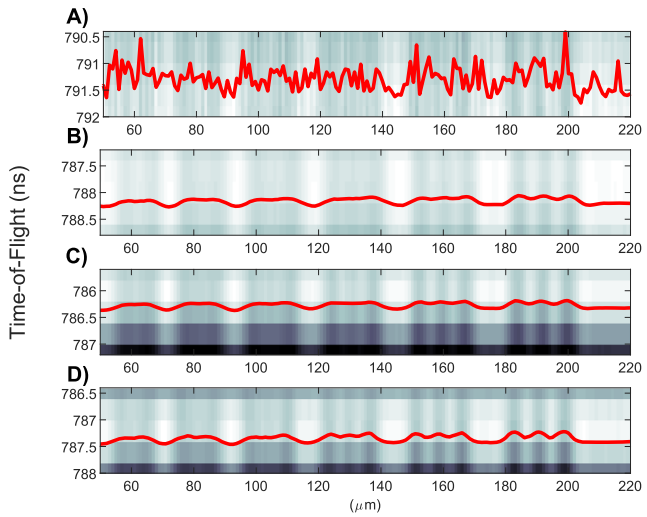

FIG. 6. Study of z-resolution of different signals. The images are B-scans (vertical lines are single A-scans) where the fitted red line follows the maximum value of the adjacent measurements: (a) traditional burst excitation at 250 MHz (six cycles), (b) linear chirp excitation (130–370 MHz; burst length, 1 μs), (c) non-linear chirp excitation (130–370 MHz; burst length, 1 μs), and (d) non-linear chirp excitation (100–450 MHz; burst length, 1 μs).

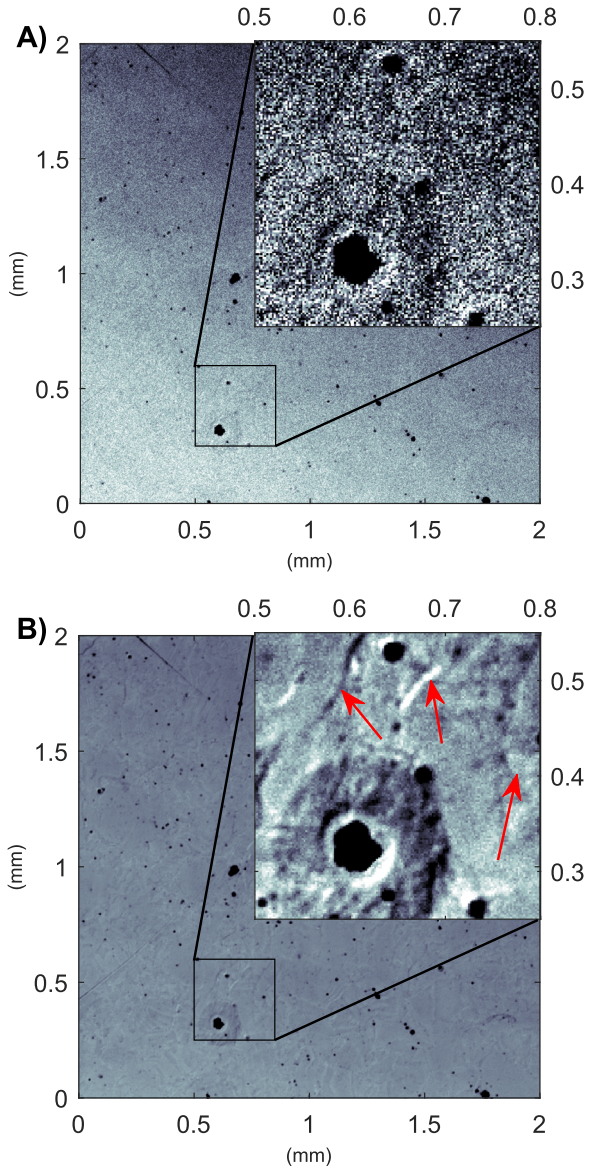

FIG. 7. Amplitude C-scan of a copper sample obtained by traditional burst excitation (a) and linear chirp excitation (b). The image quality offered by coded excitation is enhanced. See zoomed-in insets around a pit found in the sample. Note the grain boundaries that are visible in (b) (marked with arrows).

(10 min; 4 mm^2 area), the same Tx amplitude, and care that no sample motion occurs between consecutive images. Comparing image quality is nontrivial. Our focus is on improving the imaging fidelity (no distortion in line phantoms along X and Y directions) and on increasing the SNR and CNR.

We demonstrated a high-fidelity acoustic microscope. We showed that by selecting a certain code, we could enhance either the temporal resolution or the SNR (see Table III). The temporal resolution was increased by having a larger bandwidth (shorter RF pulses after pulse compression), whereas the SNR was increased by having more energy inside the frequency band of the transducer. By using a linear chirp signal, the SNR was increased [(16.3 ± 0.8) dB]. The SNR depends on the time-bandwidth product.[18] Since our linear chirp and burst excitation have similar spectra, the SNR increase is due to the longer signal (greater total energy): $10\log_{10}\left(\frac{1\ \mu s}{24\ ns}\right) = 16.2\ dB$. However, the lateral resolution was not significantly changed since the central wavelength remained the same.

We note that out signals contain a narrow train of pulses [Figs. 3(c) and 3(d)], which is caused by an electrical echo in the RF cable. This feature is visible when the bandwidth of the excitation signal is broad enough. The electrical echoing could be reduced by adding an impedance matching circuit between the RF switch and transducer. Figure 3(e) shows the absolute power spectrum density of the received signals. The burst signal is weaker than the other signals, which is caused by the short duration of the burst. However, Fig. 3(e) shows two main advantages of using coded signals: (1) The total energy of the Rx signal is higher in absolute terms than the energy in the burst signal. (2) The signal bandwidth can be tuned [broadband non-linear FM-chirp (green signal) vs other signals].

Figure 3(e) shows that the energy content at high frequencies has increased with the non-linear codes compared to the burst signal, which explains the improved resolution seen in Figs. 5 and 6. When we drove the transducer with a broad bandwidth signal using non-linear chirps, we obtained a SNR increase of 10.3 dB with a reduced echo width of 70.5% [Fig. 4(d)] and a significantly increased image quality compared to what was possible with traditional burst excitation [Fig. 4(a)]. The increase in imaging fidelity is apparent in the z-resolution (Fig. 6).

Our microscope can measure large areas with high resolution: Using the current hardware, we imaged an area of 4 mm^2 with 2 μm steps (1 Mpixel image) in 10 min with no sample preparation, as is evident in the image of the copper sample (Fig. 7). The copper sample image demonstrates the advantage of coded excitation. It is known in the literature that the grain boundaries of copper crystals [visible in the inset of Fig. 7(b)] are difficult to detect with the SAM.[23] Fast and large area imaging has advantage over other imaging modalities, such as SEM (requires a vacuum and sample coating), AFM (limited range), and fluorescence microscopy (requires sample preparation).

Our time-resolved system records the whole A-scan signal from each measurement point, which consists of 3000 samples (32 bits each after cross-correlation) that need to be analyzed, and thus, much RAM is needed. The development of computer hardware will make this limitation less impeding, and hence, larger scan areas at short measurement times should be possible in the future. To expand our instrument into GHz frequencies, our frequency doubling component needs to be changed to a frequency mixer or a modulator, as demonstrated in Refs. 22 and 24. Moving the frequency band to higher frequencies and making it broader could further enhance the resolution.

We suggest that our device may find use especially in the field of non-destructive evaluation (NDE) and biology where imaging large areas with high resolution is desired.[2,5] To upgrade an existing SAM device to employ coded excitation, one needs an AWG and a set of RF components, depending on the current system in use. The approximated cost of all components is 15 000 €, which is comparable to the cost of a new transducer.

CONCLUSION

We presented a Coded Excitation Scanning Acoustic Microscope (CESAM) that employs coded signals to achieve a high SNR and CNR (LFM: 16.3 ± 0.8 and 28.2 dB, respectively) and a reduced echo width (from 26.7% to 70.5% depending on the Tx code). This increased the imaging depth resolution and reduced the image noise compared to the case where traditional excitation was used. The microscope allows imaging fairly large areas (4 mm^2) in reasonable time (10 min).

The measurement instrument advances the state-of-the-art (see, e.g., Ref. 2) since we can optimize, case-by-case, either the CNR, SNR, or pulse width. Most importantly, we demonstrated that the use of coded signals did not distort the imaging capability of the microscope. When studying the microscope performance, we used the microscope itself as its own reference by driving it with traditional and coded signals. Since our reference samples were standard, our results can be compared to the results obtained by others in the field.

SUPPLEMENTARY MATERIAL

See the supplementary material for (1) a detailed list of used hardware, (2) a detailed description and schematic of the custom-built RF switch, (3) a description of the signal processing for RX signals, (4) the image of the distortion test for the 4 mm^2 area, and (5) a detailed analysis of amplitude comparison between burst and cross-correlated echoes.

ACKNOWLEDGMENTS

The authors gratefully acknowledge Kibero GmbH for providing the transducer.

DATA AVAILABILITY

The data that support the findings of this study are available from the corresponding author upon reasonable request.

REFERENCES

[1]R. A. Lemons and C. F. Quate, "Acoustic microscope–scanning version," Appl. Phys. Lett. **24**(4), 163–165 (1974).
[2]D. Rohrbach, A. Jakob, H. O. Lloyd, S. H. Tretbar, R. H. Silverman, and J. Mamou, "A novel quantitative 500-MHz acoustic microscopy system for ophthalmologic tissues," IEEE Trans. Biomed. Eng. **64**(3), 715–724 (2017).
[3]R. A. Lemons and C. F. Quate, "Acoustic microscopy: Biomedical applications," Science **188**(4191), 905–911 (1975).
[4]G. Vogg, T. Heidmann, and S. Brand, "Scanning acoustic GHz-microscopy versus conventional SAM for advanced assessment of ball bond and metal interfaces in microelectronic devices," Microelectron. Reliab. **55**(9–10), 1554–1558 (2015).
[5]K. Raum, K. V. Jenderka, A. Klemenz, and J. Brandt, "Multilayer analysis: Quantitative scanning acoustic microscopy for tissue characterization at a microscopic scale," IEEE Trans. Ultrason., Ferroelectr., Freq. Control **50**(5), 507–516 (2003).
[6]L. Wang, K. Maslov, J. Yao, B. Rao, and L. V. Wang, "Fast voice-coil scanning optical-resolution photoacoustic microscopy," Opt. Lett. **36**(2), 139–141 (2011).
[7]J. Chen, X. Bai, K. Yang, and B.-F. Ju, "Angular measurement of acoustic reflection coefficients by the inversion of $V(z, t)$ data with high frequency time-resolved acoustic microscopy," Rev. Sci. Instrum. **83**, 014901 (2012).
[8]J. Chen, X. Bai, K. Yang, and B.-F. Ju, "Simultaneously measuring thickness, density, velocity and attenuation of thin layers using $V(z, t)$ data from time-resolved acoustic microscopy," Ultrasonics **56**, 505–511 (2015).
[9]G. Ross, V. Vuorinen, M. Petzold, M. Paulasto-Kröckel, and S. Brand, "Gigahertz scanning acoustic microscopy analysis of voids in Cu–Sn micro-connects," Appl. Phys. Lett. **110**, 054102 (2017).
[10]O. D. Payton, L. Picco, and T. B. Scott, "High-speed atomic force microscopy for materials science," Int. Mater. Rev. **61**(8), 473–494 (2016).
[11]S. C. Minne, J. D. Adams, G. Yaralioglu, S. R. Manalis, A. Atalar, and C. F. Quate, "Centimeter scale atomic force microscope imaging and lithography," Appl. Phys. Lett. **73**(12), 1742–1744 (1998).
[12]S. Yamamizu and N. Chubachi, "Breakdown voltage and output power of ZnO piezoelectric film transducers obtained by DC diode sputtering," Jpn. J. Appl. Phys., Part 1 **15**(2), 381 (1976).
[13]R. Y. Chiao and X. Hao, "Coded excitation for diagnostic ultrasound: A system developer's perspective," in *2003 IEEE International Ultrasonics Symposium* (IEEE, 2003), Vol. 1, pp. 437–448.
[14]M. Nikoonahad, G. Q. Yue, and E. A. Ash, "Pulse compression acoustic microscopy at 750 MHz," Electron. Lett. **19**(19), 782–784 (1983).
[15]X. Song *et al.*, "Coded excitation speeds up the detection of the fundamental flexural guided wave in coated tubes," AIP Adv. **6**(9), 095001 (2016).
[16]M. Pollakowski and H. Ermert, "Chirp signal matching and signal power optimization in pulse-echo mode ultrasonic nondestructive testing," IEEE Trans. Ultrason., Ferroelectr., Freq. Control **41**(5), 655–659 (1994).
[17]B. Wang, J. Wang, X. Song, and F. Liu, "Q-learning-based adaptive waveform selection in cognitive radar," Int. J. Commun., Network Syst. Sci. **2**(7), 669–674 (2009).
[18]M. O'Donnell, "Coded excitation system for improving the penetration of real-time phased-array imaging systems," IEEE Trans. Ultrason., Ferroelectr., Freq. Control **39**(3), 341–351 (1992).
[19]A. Habib and F. Melands, "Chirp coded ultrasonic pulses used for scanning acoustic microscopy," in *2017 IEEE International Ultrasonics Symposium (IUS)* (IEEE, 2017), pp. 1–4.
[20]A. Habib, J. Vierinen, A. Islam, I. Z. Martinez, and F. MelandsØ, "Vitro volume imaging of articular cartilage using chirp-coded high frequency ultrasound," in *2018 IEEE International Ultrasonics Symposium (IUS)* (IEEE, 2018), pp. 1–4.
[21]M. Nikoonahad, G.-Q. Yue, and E. A. Ash, "Pulse compression acoustic microscopy using SAW filters," IEEE Trans. Sonics Ultrason. **32**(2), 152–163 (1985).
[22]A. I. Meriläinen, T. Fabritius, J. Eskelinen, and E. Hæggström, "Solid state switch for gigahertz coded signal ultrasound microscopy," Electron. Lett. **49**(3), 169–170 (2013).
[23]M. G. Somekh, G. A. D. Briggss, and C. Ilett, "The effect of elastic anisotropy on contrast in the scanning acoustic microscope," Philos. Mag. A **49**(2), 179–204 (1984).
[24]A. Rantamaa, J. Hyvönen, A. Meriläinen, A. Salmi, and E. Hæggström, "Optimized signal generation circuit for coded GHz acoustic microscope," in *2019 IEEE International Ultrasonics Symposium (IUS)* (IEEE, Glasgow, United Kingdom, 2019), pp. 2000–2002.